Scientific Report SAC/EPSA/CVD/CAL-VAL/03/2017

The absolute vicarious calibration of VIS and SWIR channels of INSAT-3D and INSAT-3DR over desert sites

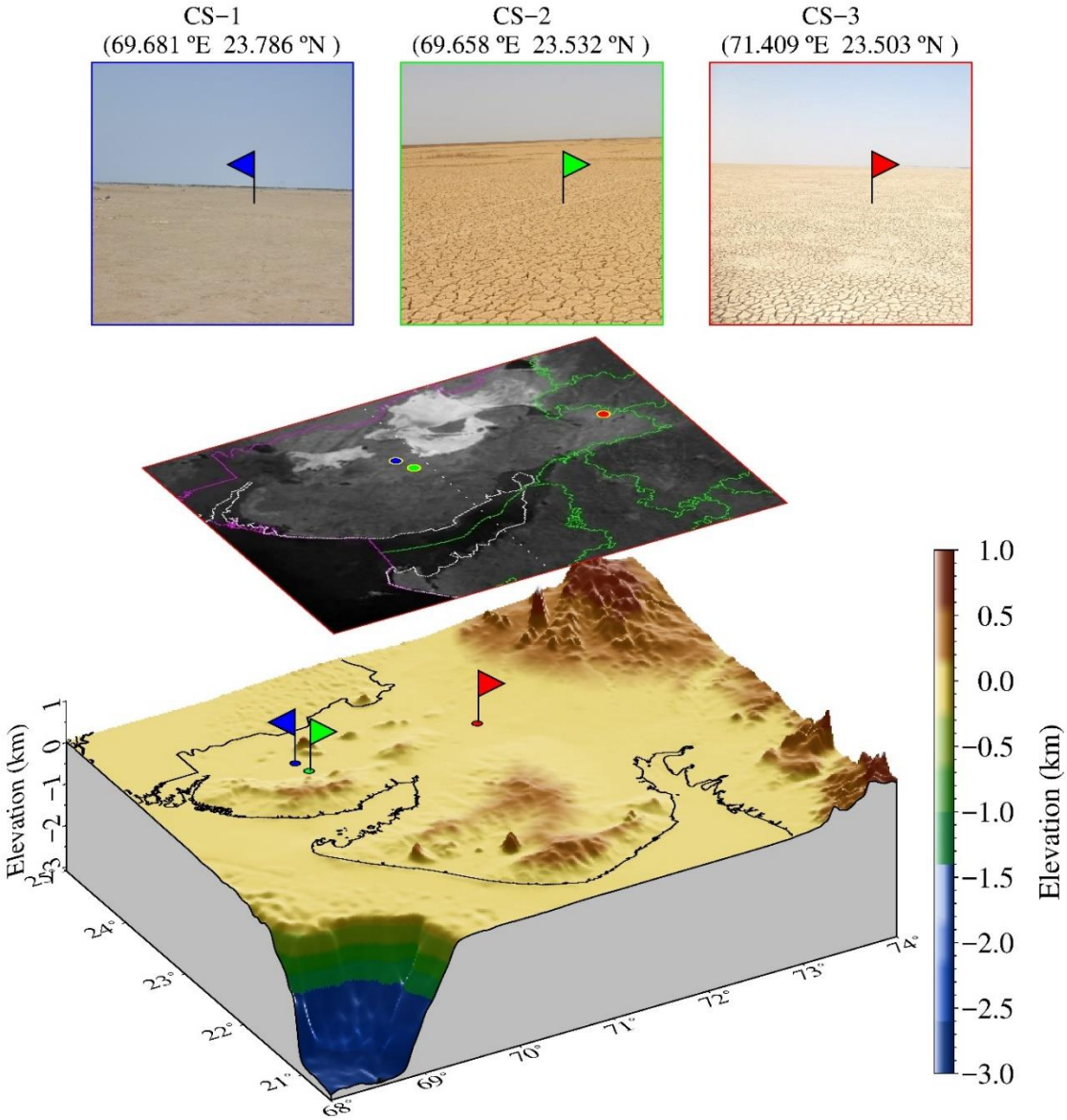

Piyushkumar N. Patel, K N Babu, R P Prajapati

and A K Mathur

Calibration-Validation Division (CVD)
Earth, Ocean, Atmosphere, Planetary Sciences & Applications Area (EPSA)
Space Applications Centre (ISRO)
Ahmadabad – 380 015

Document control sheet

1. Report No.	SAC/EPSA/CVD/CAL-VAL/2017/003
2. Publication Date	March, 2017
3. Title	The absolute vicarious calibration of VIS and SWIR channels of INSAT-3D and INSAT-3DR over desert sites
4. Type of Report	Scientific
5. Number of pages	26
6. Number of references	37
7. Authors	Piyushkumar N Patel, K N Babu, R P Prajapati and A K Mathur
8. Originating unit	CVD/EPSA
9. Abstract	This document describes the radiometric vicarious calibration of VIS and SWIR channels of INSAT-3D and INSAT-3DR over the three different desert sites.
10.Key Words	Vicarious calibration, TOA spectral radiance, INSAT-3D, INSAT-3DR
11.Security classification	Unrestricted
12.Distribution statement	Among all concerned

Contents

Abstract

The absolute radiometric calibration of a satellite sensor is the critical factor that ensures the usefulness of the acquired data for quantitative applications on remote sensing. We describe here the results of in-orbit radiometric calibration of the visible (VIS) and shortwave infrared (SWIR) bands INSAT-3D and INSAT-3DR imager, based on the ground data at three different desert sites during clear-sky conditions. These calibration activities are performed to account for the characterisation errors or undetermined post-launch changes in sensor performance. We had measured the surface reflectance and atmospheric variables at the site synchronising with the viewing and solar geometry of both the satellite scan. Top of the atmosphere (TOA) spectral radiances are computed using 6SV (Second Simulation of the Satellite Signal in the solar Spectrum) radiative transfer (RT) code with the surface reflectance and atmospheric variables as well as spectral response function (SRF) of individual channel. The derived vicarious calibration coefficients are 1.005 and 1.088 for VIS and SWIR of INSAT-3DR, respectively, while it is 1.277 and 0.903 for VIS and SWIR of INSAT-3D. The results show a significant change in VIS and SWIR bands of INSAT-3D which is suggested to be incorporated in generating next level of data products. Along with the analysis results, the uncertainties in computed calibration coefficients due to various parameters are also provided.

1. Introduction

The Indian National Satellite (INSAT)-3D/-3DR, developed by the Indian Space Research Organization (ISRO), were launched on 26th July 2013 and 8th September 2016, respectively. The former one was launched from Kourou, French, Guyana using an Ariane 5 ESA launch vehicle, whereas later one was launched using a Geosynchronous Satellite Launch Vehicle (GSLV) MK-II from SDSC-SHAR, ISRO. INSAT-3D and INSAT-3DR satellite series equipped with a 6-channels Imager and 19- channels atmospheric sounder, which operate in visible to thermal infrared region of the electromagnetic spectrum. Imager from both the satellites operate from a geostationary altitude 36000 km in visible (VIS) and shortwave infra-red (SWIR) bands with 1 km spatial resolution, while Mid-Wave Infra-Red (MWIR), Thermal Infra-Red-1 (TIR1), Thermal Infra-Red-2 (TIR2) and Water Vapor (WV) bands with 4 km spatial resolution respectively. However, sounder from INSAT-3D/-3DR has 18 infrared (IR) channels ranging from 3.7 to 14.7 µm and one visible channel for the daytime cloud detection with 10 km spatial resolution. The significant improvements incorporated in INSAT-3DR are: (1) Imaging in MWIR band to provide nighttime pictures of low clouds and fog and (2) Imaging in the split band TIR channel with two separate windows (10.2-11.2 and 11.5-12.5 micrometre regions) with 4 km spatial resolution provides estimation of sea surface temperature with better accuracy. Imager from both the satellites provide data at every 30 minutes intervals with 15 minutes difference, which means that data sets are available at every 15 minutes intervals collectively. Details about wavelength range and spatial resolution of Imager are given in Table-1.

Table 1: *Image of INSAT-3D/3DR specifications*

Band No.	Wavelength (µm)	Resolution (km)
1	VIS (0.55-0.75)	1
2	SWIR (1.55-1.70)	1
3	MWIR (3.8-4.0)	4
4	WV (6.5-7.1)	8
5	TIR-1 (10.2-11.3)	4
6	TIR-2 (11.5-12.5)	4

The primary purpose of the INSAT-3D/-3DR mission, which is a continuation of the INSAT-3A and KALPANA-1 geostationary satellite programs, is to meet the nation's need for meteorological and oceanic monitoring applications, television broadcasting, telecommunications and search and rescue services. INSAT-3D/-3DR is an advanced weather satellite of India configured with improved imaging system and atmospheric sounder as compared to earlier missions. To accomplish the suggested mission purposes, especially for quantitative applications, the potential user groups require reliable radiometric information.

Monitoring the radiometric characteristics of satellite sensors is an essential step in the estimation of reliable, continuous variables for quantitative applications. This radiometric calibration, which converts the electronic digital number (DN) values to physical units, has been performed to acquire consistently accurate radiometric information over a specifically designed sensor's life-time [1],[2]. To secure radiometric calibration and the continuity of satellite data from multiple sensors, pre- and post-launch calibration has been proposed to

determine the characteristics of radiometric calibration [3]–[5]. The pre-calibration step, which is conducted in a controlled laboratory setting, uses a well-characterized radiant source. However, because calibrated sensors are degraded by the severe environmental conditions encountered after launch [6], operational space-borne satellites need to be monitored to obtain their absolute radiometric characteristics when in orbit. For in-flight calibration of satellites, on-board, vicarious, lunar, and cross-calibration techniques have been suggested for radiometric calibration [7]–[12]. On-board calibration is performed in orbiting satellites using well-known sources such as artificial lamps or the sun. On-board calibrators have the advantage of allowing frequent response determinations. However, they increase the cost and weight of instruments. Vicarious and cross-calibration techniques are used for systems without on-board calibrators. These techniques also act as a validation tool for systems with on-board calibrators [9], [10], [13].

In this paper, the vicarious calibration method, relying on *in-situ* characterisations of surface targets, was applied to monitor the radiometric characterisations of INSAT-3D/-3DR. The radiometric characteristics of INSAT-3D was previously defined using same vicarious calibration approach by Patel et al., in 2014 and 2015 [14], [15]. However, it is necessary to monitor the radiometric characteristics of sensor in a continuous manner, to provide a better data accuracy. After a period of time the vicarious calibration activities are performed to monitor the radiometric characteristics of both INSAT-3D/-3DR. Furthermore, it is difficult to obtain atmospheric and surface measurements during the early operational period. Eventually, field campaigns are conducted over different desert sites in Little Rann of Kutch (LROK) and Great Rann of Kutch (GROK), to obtain hyperspectral surface reflectances using handheld radiometric instruments. Several important environmental conditions are necessary, such as characterizations without cloud cover and a flat homogeneous surface to derive very consistent calibration coefficients. Other input parameters are also collected for the radiative transfer model simulation (e.g., atmospheric constituents, such as aerosol optical depth, ozone column, and water vapour content) using well calibrated MicroTOPS-II sunphotometer and ozonemonitor during the field campaigns. The vicarious calibration methodology using Second Simulation of the Satellite Signal in the Solar Spectrum Vector Version (6SV) radiative transfer simulations, based on measured atmospheric parameters, is effective for practical, rapid and low-cost radiometric calibration. The aim of our study is to characterize INSAT-3D/3DR absolute radiometric calibration.

1.1. INSAT-3D/-3DR Radiance Calculation

INSAT-3D/-3DR standard full disk Level 1B data product [16] has been used in the present study. The Level 1B data is available at Meteorological and Oceanographic Satellite Data Archival Centre (MOSDAC) (www.mosdac.gov.in). INSAT-3D/-3DR measured brightness values received in terms of a digital number (DN) for each band are converted to TOA spectral radiance L(λ) values either using the lookup table or using the calibration coefficients. The look up table (LUT) provides mapping from DN to corresponding radiance values. The LUT is generated using calibration coefficients, which are provided as a filed name "Radiometric_Calibration_Type" in the data product as attribute. Lab and online radiometric calibration coefficients are available as part of attribute in the data product, which can be used for computing radiance directly from DN. Lab coefficients are provided in terms of slope, offset and quadratic term in the provided product, which are generated using pre-launch ground test data. Whereas online calibration is performed using on-board internal blackbody serving

as a hot target and space view count as cold target, which provides two online slope and offset values. Quadratic term is derived using inter sensor calibration. More details about the procedures for both the calibration coefficients are given in the INSAT-3D/-3DR data products format document, 2014 [16]. While estimating the radiance values the DNs should be inverted, if a field name "invert"=true in the attribute indicates the image DNs are inverted. The coefficients
provided for DN to radiance conversion are used as follows:

$$DN_{inv} = DN_{max} - DN \ (only\ if\ \text{invert} = true) \quad (1)$$

Where DN_{inv} is the inverted DN value. DN_{max} = 1023 for imager.

$$L(\lambda)(in\ mw\ cm^{-2}sr^{-1}\mu m^{-1}) = lab/online\_radiance\_quad \cdot (DN)^2 + lab/online\_radiance\_scale\_factor * DN \quad (2)$$

Here, DN is digital numbers recorded by the sensor. The values for the slope (scale factor), offset and quadratic term to convert DN to radiance for each band are provided in the attribute.

2. Test sites and field measurements

2.1. Calibration Site (CS)

Attributing to their preferable stability of surface characteristics and atmospheric dynamics, pseudo invariant sites are commonly used for sensor radiometric calibration, degradation monitoring and inter-comparisons [17], [18] especially for the satellite sensors without on-board calibration facilities. The Committee on Earth Observation Satellites (CEOS) Working group on Calibration and Validation identified several test sites around the world [19] based on the selection criteria, such as low probability of atmospheric variability, high spatial homogeneity, weak directional effects, flat reflectivity spectrum. Calibration sites are never chosen randomly, and to be adequate they must satisfy a certain number of criteria [20]-[23]. Based on these criteria, we have selected two desert sites in Great Rann of Kutch (GROK) and one in Little Rann of Kutch (LROK) in Gujarat, India. Fig.-1 shows the map of all three calibration sites and their locations indicated by flags and the associated photographs of the sites. Following are the detail of the calibration sites:

Calibration Site-1 (69.681 ºE, 23.786 ºN):

Calibration Site (CS)-1 is located near Khavda village on the way of white desert, Gujrat with an altitude of ~4 meter above the mean sea level. The site is extended upto ~6 km^2 area, presenting a flat and homogenous terrain characterized by a low reflectance surface with high soil moisture content due to excessive water logging during the monsoon season, the soil wetness decreases with time and completely dried in pre-summer and summer season.

Calibration Site-2 (69.658 ºE, 23.532 ºN):

CS-2 is placed between Loriya and Bhirandiyara villages in GROK, Gujarat. The site is mostly covered by barren agriculture land, which is dominated by dry land and little shrubs

at few parts. The site is extended upto ~20 km^2 area covered with the small hills in southern side of the site.

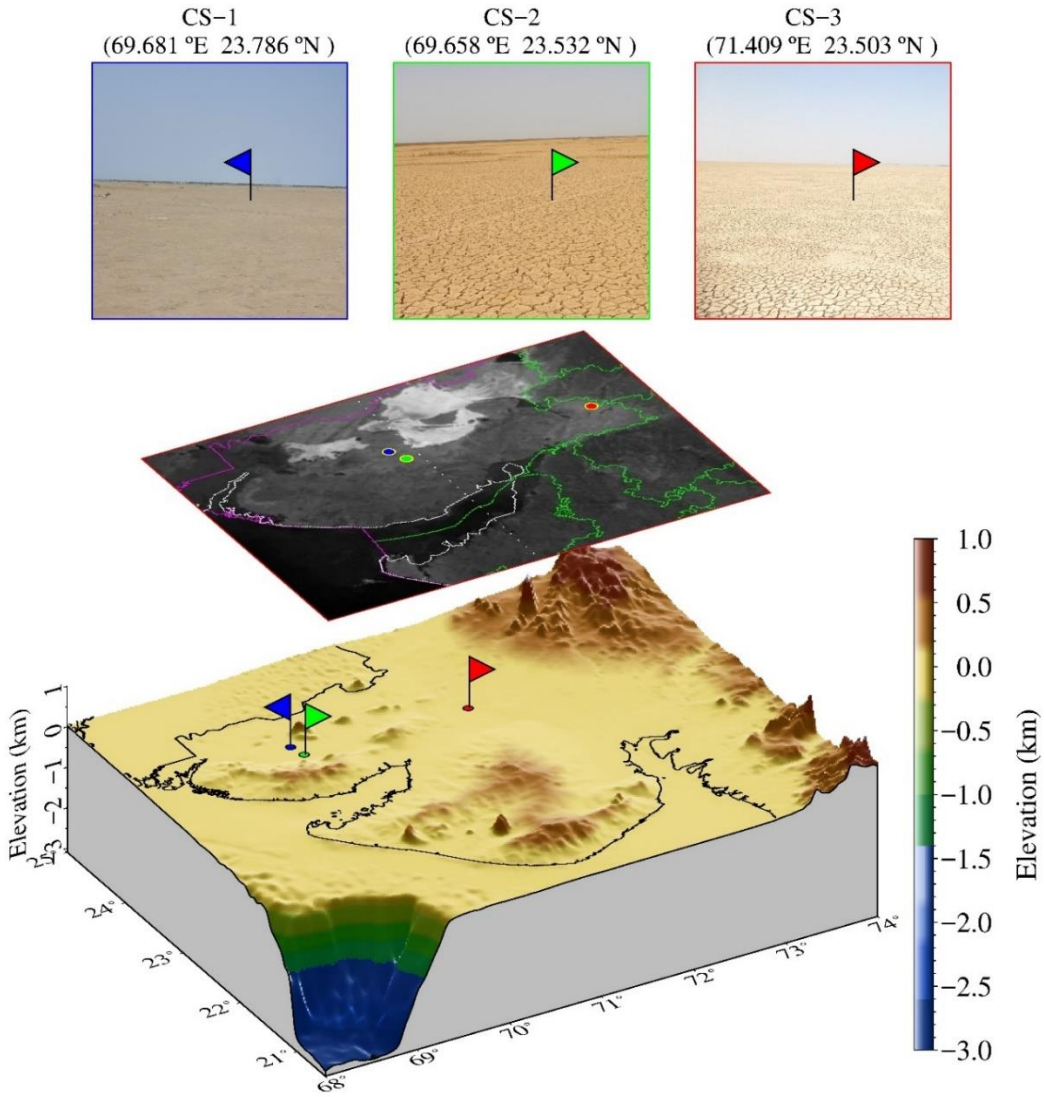

Figure 1: *Map of calibration site (CS)s used in the present study for the measurements of surface reflectance and atmospheric parameters to simulate TOA spectral radiance for the calibration of INSAT-3D/-3DR. Flags in bottom panel show the location of calibration sites. Middle panel illustrate the location of calibration sites in INSAT-3DR VIS image. Top panel shows the site photographs of calibration sites: (1) CS-1 (blue): near Khavda, GROK, Gujarat (69.681 ºE, 23.786 ºN) (2) CS-2 (green): near Loriya, GROK, Gujarat (69.658 ºE, 23.532 ºN) (3) CS-3 (red): near Amarapur, LROK, Gujarat (71.409 ºE, 23.503 ºN).*

Calibration Site-3 (71.409 ºE, 23.503 ºN):

CS-3 is a complete deserted site in Little Rann of Kutch (LROK), Gujarat with an altitude of ~6 m above mean sea level. This site is extended more than 60 km^2 area, presenting a completely flat and homogenous terrain characterized by high surface reflectance. The area is a vast, homogenous, plain land with mostly dry, salty soil dominating the landscape during the months of December to May, and prone to excessive water logging during the monsoon season (June – September). The site is a clay-dominated dry land with different spectral

characteristics that have been used for radiometric calibration sites for large footprint sensors (e.g. INSAT-3A, INSAT-3D and INSAT-3DR).

2.2. Field Campaign

We performed field campaigns for vicarious calibration of INSAT-3D/-3DR at three test sites during 2016 and 2017. As described in section 2.1 all three sites are clay-dominated dry lakes with different spectral characteristics that have been used for radiometric calibration of satellite sensors [15]. Simultaneous observations from satellite and ground have been successfully conducted at different dates as shown in table-2. On ground data are collected between 04:30 UTC and 08:00 UTC to cover maximum possible satellite overpass with the suitable atmospheric conditions.

Table 2: *The date and time of ground data collection at the associated calibration site and the covered INSAT-3D/-3DR imageries.*

Date	Calibration Site (No. of pass covered 3D/3DR)	INSAT-3D overpass (UTC/IST)	INSAT-3DR overpass (UTC/IST)
09-11-2016	CS-1 (5/5)	05:00/10:30 05:30/11:00 06:00/11:30 06:30/12:00 07:00/12:30	05:15/10:45 05:45/11:15 06:15/11:45 06:45/12:15 07:15/12:45
31-01-2017	CS-3 (3/4)	06:00/11:30 06:30/12:00 07:00/12:30 -	05:45/11:15 06:15/11:45 06:45/12:15 07:15/12:45
07-02-2017	CS-2 (6/5)	04:30/10:00 05:00/10:30 05:30/11:00 06:00/11:30 06:30/12:00 07:00/12:30	04:45/10:15 05:15/10:45 05:45/11:15 06:15/11:45 06:45/12:15 -
08-02-2017	CS-2 (2/2)	05:30/11:00 06:00/11:30	05:15/10:45 05:45/11:15
09-02-2017	CS-2 (6/6)	05:00/10:30 05:30/11:00 06:00/11:30 06:30/12:00 07:00/12:30 07:30/13:00	04:45/10:15 05:15/10:45 05:45/11:15 06:15/11:45 06:45/12:15 07:15/12:45
06-03-2017	CS-3 (6/7)	05:00/10:30 05:30/11:00 06:00/11:30 06:30/12:00 07:00/12:30 07:30/13:00 -	04:45/10:15 05:15/10:45 05:45/11:15 06:15/11:45 06:45/12:15 07:15/12:45 07:45/13:15

The ground measurements over target areas (CS-1: 2x2 km, CS-2: 4x4 km, CS-3: 6x6 km) have been measured near-simultaneously at the time of INSAT-3D/-3DR overpass. Data are collected in zigzag manner in CS-3 as described by Patel et al., 2015 [15], while the measurements are carried out randomly at almost every 500 m distance over other sites (CS-1 and CS-2).

2.3 Atmospheric Measurements

Since the algorithm employed radiative transfer calculations in the atmosphere, the specification of atmospheric conditions is necessary including the thermodynamic condition. However, we have measured aerosol optical depth (AOD), total columnar ozone (TCO) and total water vapour content (WVC) during field campaign. AOD measurements are carried out using a multi wavelength MicroTops-II sun-photometer (M/s. Solar Light Co., USA) at five different wavelengths at 380, 440, 500, 675 and 870 nm, from the solar instantaneous flux measurements with its internal calibration using the Langley method [24], [25]. The Full Width at Half Maximum (FWHM) bandwidth for the 380 nm channel is 2.4 ± 0.4 nm and 10 ± 1.5 nm for the other channels [26].

Table 3: *Daily mean values of aerosol optical depth at 500nm, Total column Ozone and Water Vapour content*

Date (site)	AOD at 500 nm	Total column ozone (DU)	Water Vapour Content (g cm^{-2})
09-11-2016 (CS-1)	0.219	274	0.79
31-01-2017 (CS-3)	0.277	278.7	0.65
07-02-2017 (CS-2)	0.205	255.2	0.36
08-02-2017 (CS-2)	0.355	249.3	0.63
09-02-2017 (CS-2)	0.185	262.1	0.30
06-03-2017 (CS-3)	0.374	270.0	0.69

A MicroTops-II Ozonometer, a ground-based instrument, which is capable of measuring the column ozone (CO) using three UV channels (305.5, 312.5, 320.0 nm) and the total water vapour content (WVC) using two near-IR channels (940 and 1020 nm) [27] as well as AOD at 1020 nm is also used during the field campaigns. More details of design, performance, error and calibration of MicroTops-II is given elsewhere [26], [27]. Table-3 shows the daily mean values of AOD at 500 nm, CO and WVC for all the measurement days over all three calibration sites.

2.4 Surface Reflectance

Measurements of ground reflectance are carried out using a portable hyperspectral radiometer (FieldSpec-3 of M/s. Analytical Spectral Devices (ASD), Inc., 350-2500 nm), in a predetermined pattern so that the pixel averaging can be performed. The fore-optic for light collection is projected out using a camera monopod to avoid the measurement noise, thereby ensuring that the surface being measured and free from shadows. The main unit is carried in a backpack, and the computer is carried on platform in front of the user. The reference measurements using Spectralon white plate are made at predetermined interval throughout the

site collection. The ASD FieldSpec 3 has a 3-nm spectral resolution covering 350–1000 nm and a 10-nm spectral resolution in the 1000–2500 nm spectral range. To consider changeable light field conditions, optimization adjustments, dark correction, and white reference scan are conducted to obtain reliable target reflectance. All of the surface reflectance measurements are carefully processed. Fig.-2 shows the daily mean measured surface reflectance over all three sites along with standard deviation (at 1σ level). Water vapour absorption at 1380 nm and 1800 nm are the major reasons for the two gaps in the reflectance curves. These curves describes the different soil characteristics of the calibrations sites. The mean reflectance values measured on 7 and 8 February 2017 over CS-2 are very similar, but very small coverage of very thin cirrus clouds at high altitude reduce the magnitude of reflectance compared to 9 February. Similar to this, a mean reflectance spectrum on 6 March over CS-3 is greater than 31 January caused by the surface humidity at the calibration site, because water logging during summer monsoon period over CS-3 increase the surface wetness and it becomes dry over a period.

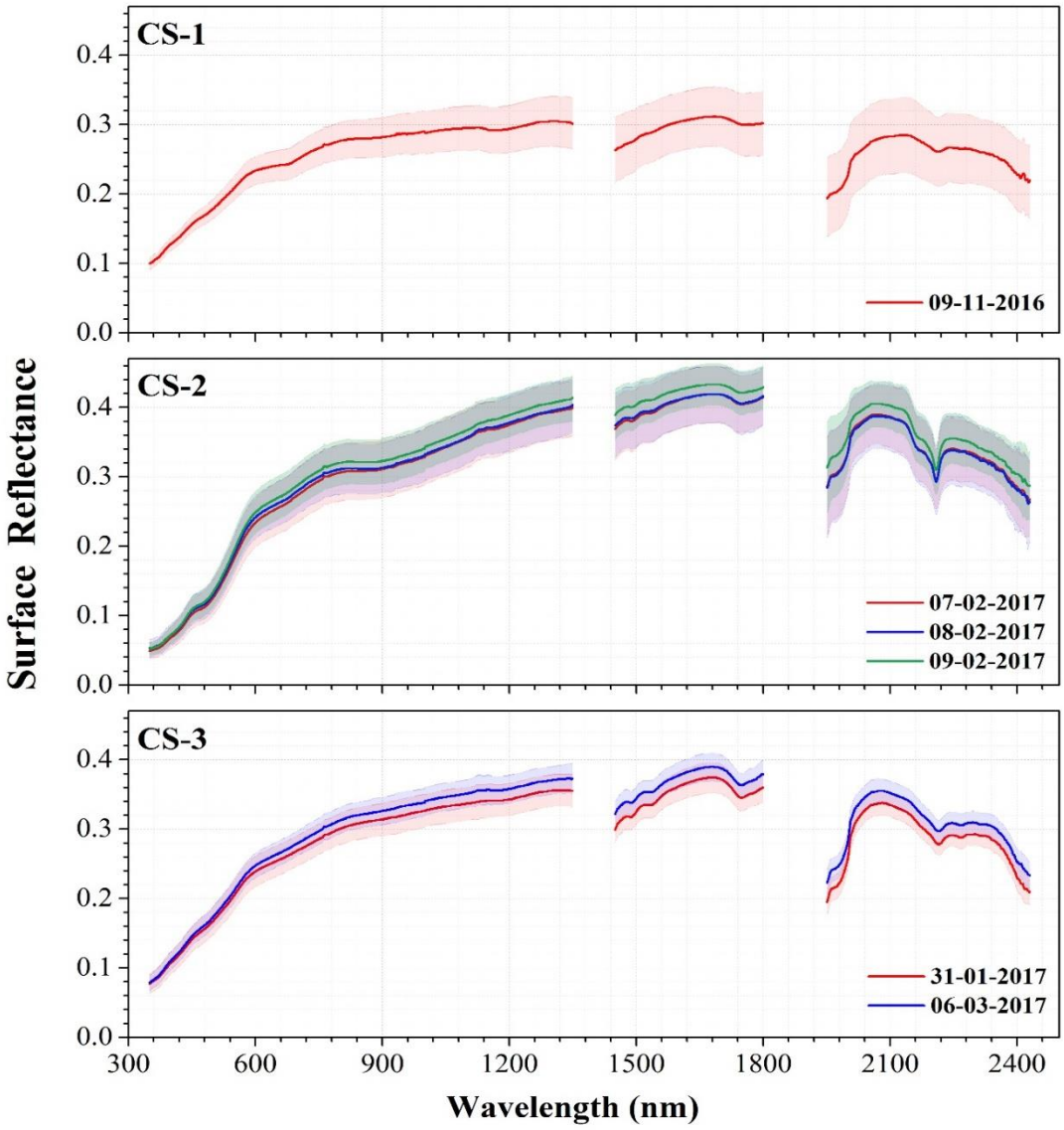

Figure 2: *Daily mean surface reflectance at all three calibration sites along with standard deviation (1σ level).*

Fig.-3(a) shows the mean surface reflectance along with standard deviation at 1σ level. The average reflectance curve of CS-3 is uniform across the spectrum and show very little variation compared to other two calibration sites. Considering the INSAT-3D/-3DR VIS bands, the surface reflectance curves of CS-2 and CS-3 are similar and greater than CS-1. However, the surface reflectance in SWIR bands shows the high values over CS-2 followed by CS-3 and CS-1, which may be caused by a contamination of surface wetness that may differ with time.

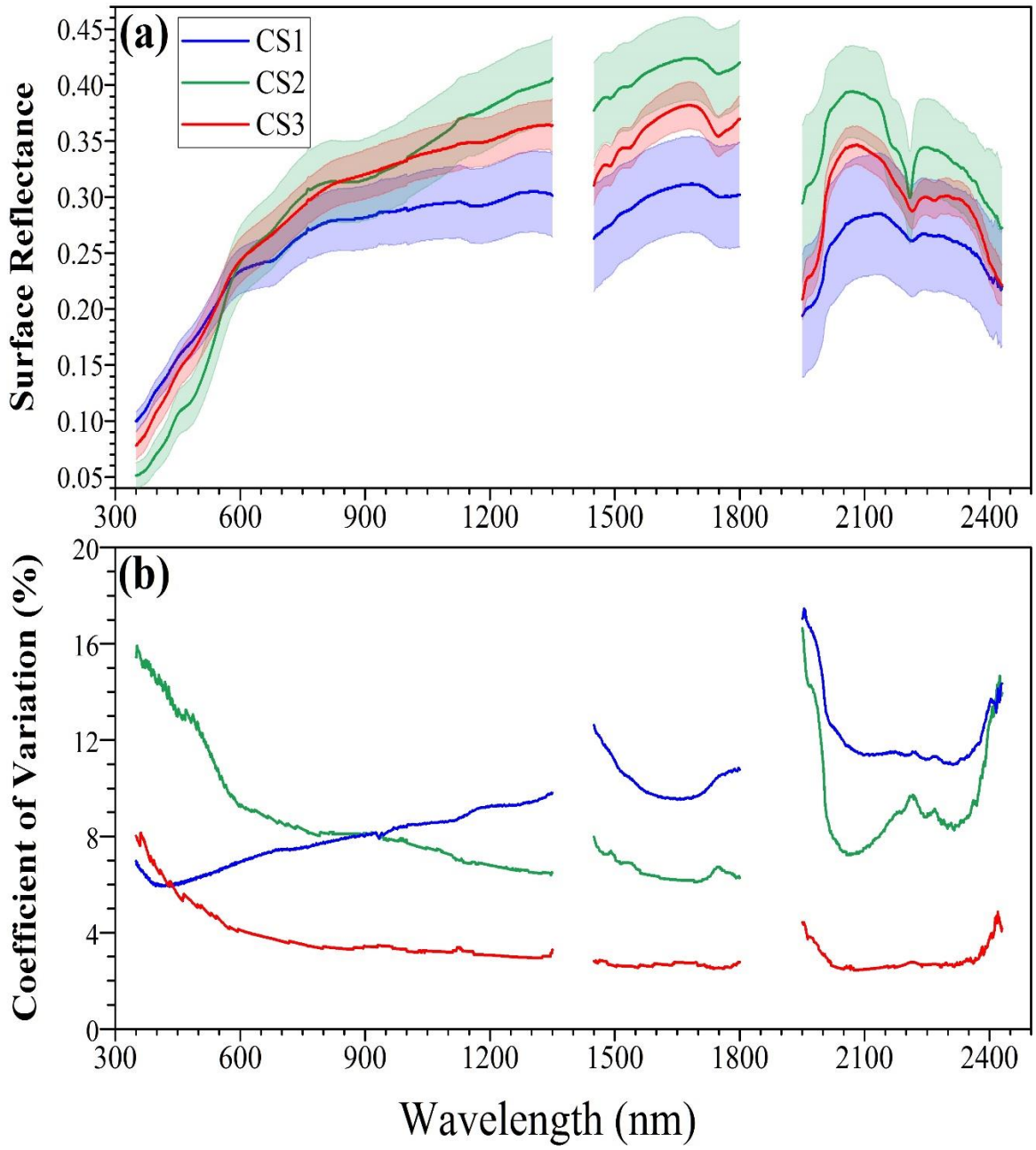

Figure 3: *(a) Mean surface reflectance along with standard deviation at 1σ level. (b) Coefficient of Variation (CV) in percentage of all three calibraiton sites.*

CS-2 shows the high variation (large standard deviation) as compared to other two sites in VIS band, while in SWIR band, CS-1 shows the large value of standard deviation. This is clearly describe in the analysis of coefficient of variation (CV (%) = (standard deviation / mean)*100) in Fig.-3(b). CV analysis shows the CS-3 is highly uniform site compared to CS-1 and CS-2 in both VIS (~3.9%) and SWIR (~3.0%) bands, while CS-2 shows large variation with CV value of ~9.1% in VIS and 6.9% in SWIR, CS-3 shows the large variation in SWIR with CV=~10.2% and 7.1% in VIS.

3. Methodology

Reflectance-based and radiance-based techniques are the most common approaches when in-situ data are used to calibrate satellite sensors [22]. Reflectance-based technique is used in this study, because it is difficult to maintain the radiometric accuracy of the spectrometer that measures the surface radiance in the radiance-based technique. The reflectance-based technique mainly depends on the measured ground surface reflectance. The reflectance is characterized by the ratio of measurement of the site to those of a standard reflectance/ Spectralon panel for which the bidirectional reflectance factor is precisely determined. The vicarious radiometric calibration depends on the surface reflectance and radiance from the sun to earth's surface and earth's surface to sensor and atmospheric optical thickness over the calibration site at the time of satellite pass. The ground measurements are used as an input for radiative transfer (RT) code for the simulation of absolute radiances in the required bands at the sensor level. The ground measurements are used to define the spectral directional reflectance of the surface and the spectral optical depth that are used to describe the aerosol and molecular scattering effect in the atmosphere [28] along with this we used columnar water vapour to include the water vapour absorption effect. We have used improved 6SV RT code [29], [30] to compute the radiance field using ground measurements. 6SV RT code predicts the satellite signal at TOA level using ground reflectance measurements and atmospheric measurements of sunphotometer. 6SV RT model is a physically based model, which is not specified for particular satellite or test sites. Because of that 6SV RT model is used for this study. In addition, 6SV RT model has spectral libraries for gaseous absorption and scattering by aerosols and molecules. 6SV deals better with atmospheric scattering than other RT models [31]. 6SV model was formulated for the atmospheric correction in the short wavelengths. 6SV code requires the geometric conditions, including the viewing zenith, viewing azimuth, solar zenith and solar azimuth angles. Viewing zenith and viewing azimuth angles are obtained from satellite metadata files and solar zenith and solar azimuth angles are calculated using time and location for a given data point.

Fig.-4 describes with flow diagram the simulation of TOA spectral radiance and estimation of calibration coefficient. For the RT simulation to derive the vicarious calibration coefficient, the optimum selection of aerosol type is important. The actual aerosol characteristics are often differing from standard aerosol models in the RT codes. It is difficult to precisely estimate the aerosol characteristics in the field campaign. This leads to the systematic errors in the calibration results [37]. However, in the present study we have used handheld MicroTops-II sunphotometer for the measurements of AOD. This cannot provide other optical and physical properties of aerosols (e.g. volume size distribution, refractive indices etc.), which helps to improvise the aerosol parameterization in the RT model and leads to high accuracy of TOA spectral radiance simulation. However, due to lack of measurements, we have considered the

continental aerosol model as a better representation of aerosol over calibration sites, which is the basic model over the land site.

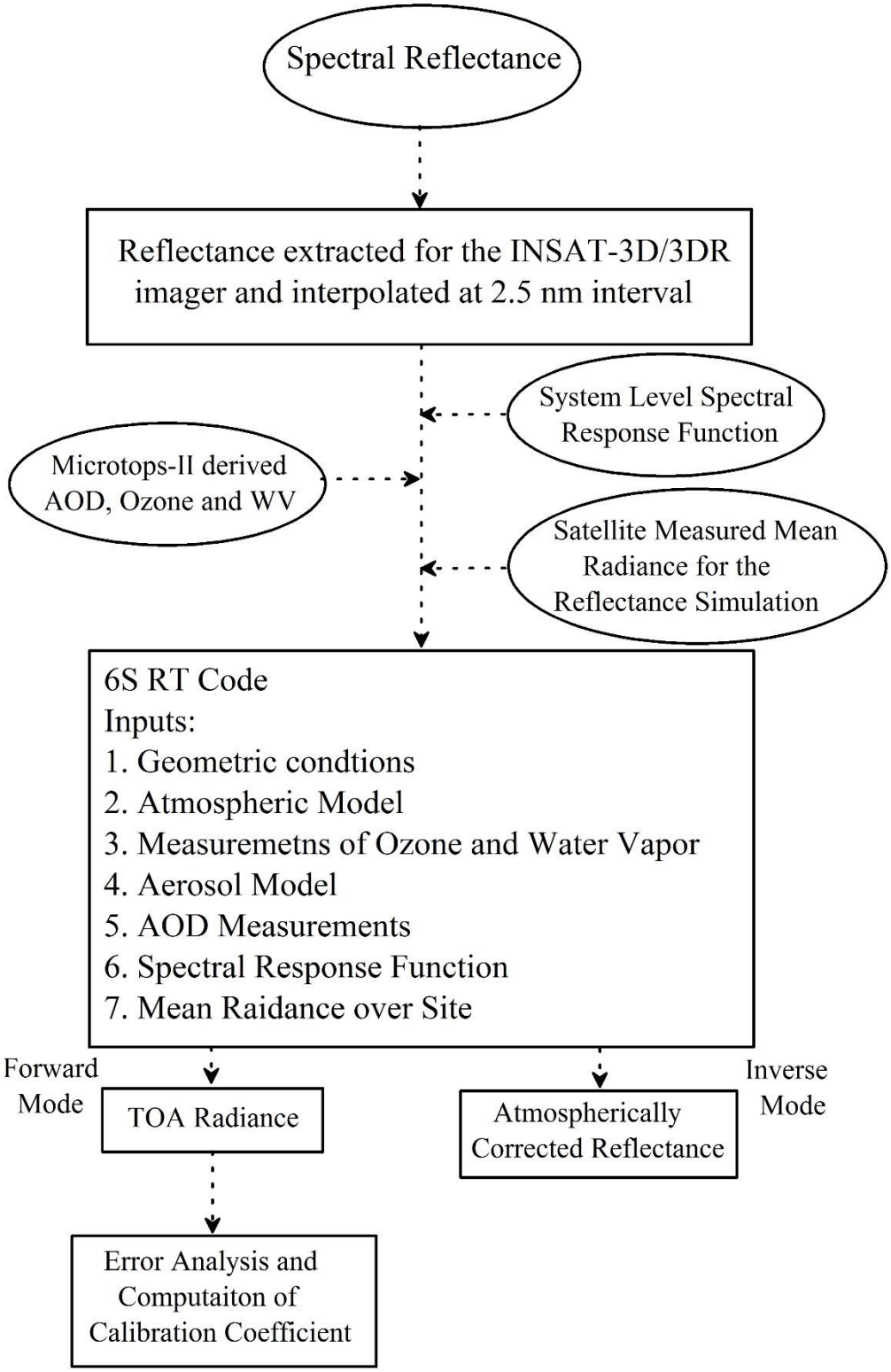

Figure 4: *Flow chart of TOA spectral radiance simulation and estimation of calibration coefficient.*

Additionally, to reflect the characteristics of INSAT-3D/-3DR spectral bands, the normalized spectral response function (SRF)s are also used as inputs in the 6SV RT model (Fig.-5) to simulate the TOA spectral radiance.

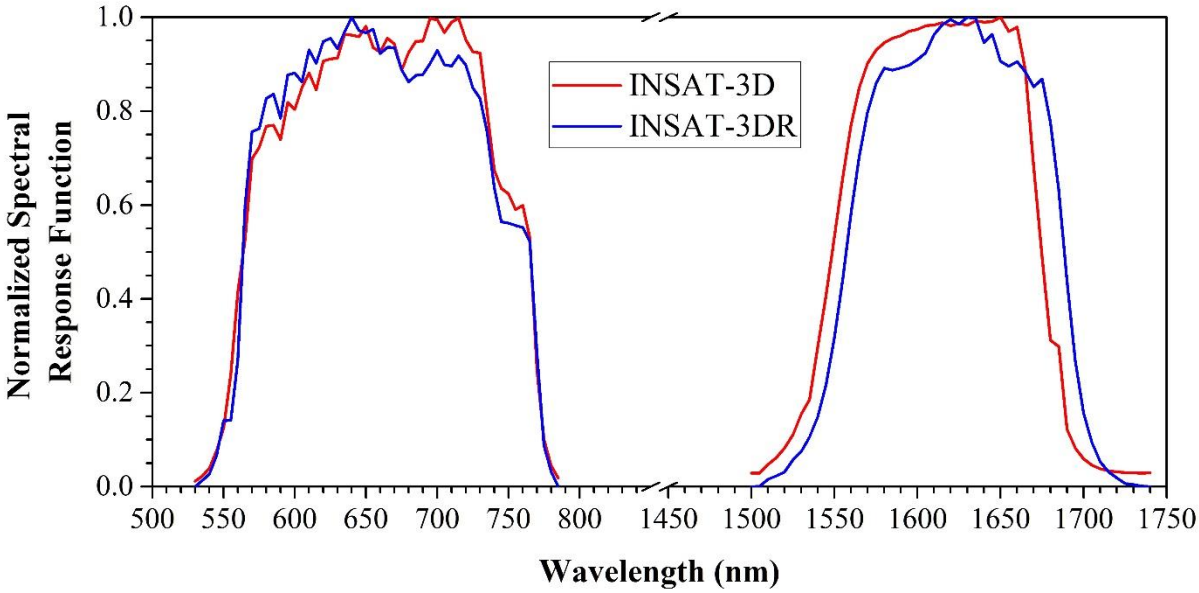

Figure 5: *Pre-launch laboratory measurements of spectral response function of VIS and SWIR channels of both INSAT-3D/-3DR.*

Both the SRF and measured surface reflectance data are resampled to 2.5 nm intervals using a spline interpolation method. The 6SV RT model computes TOA spectral radiance in the forward mode, while it computes atmospherically corrected surface reflectance in the inverse mode. 6SV RT model provides an output in the form of TOA spectral radiance, which is divided by the corresponding radiance observed by the INSAT-3D/-3DR for particular channel to yield calibration coefficients.

3.1 BRDF effect

Surface albedo is related to surface reflectance which depends on the bidirectional reflectance distribution function (BRDF), which indicates the dependence of reflectance on solar and viewing geometry [32]. In general, reflectance of light is an anisotropic phenomenon and this anisotropy is very small compared to Lambertian component except at special geometries like specular reflection from water surface. The precise computation of surface reflectance requires the anisotropy estimation. The BRDF effect provides a precise computation of uncertainty in reflectance arising due to the neglecting anisotropy. In the present study, the calibration test sites can be reasonably assumed as Lambertian; therefore, the effect of BRDF is not considered in our simulation [33], but the error associated due to incomplete measurements of BRDF over the calibration sites is estimated using MODIS derived BRF product. We used combined MODIS Terra and Aqua BRDF product (MCD43A1), to compute the effects of surface anisotropy on TOA spectral radiance. The MCD43A2 data product [34] provides high quality three Ross-Li BRDF model parameters (isotropic, volume scattering and geometric optical reflectance terms), which are pixel-wise

implemented into 6SV RT model to estimate BRDF effect. We used approximately common bands for MODIS and INSAT-3D/-3DR. MODIS provides BRDF coefficients in the seven narrow bands and three broad bands. We have used MODIS first broad band (0.4–0.7 mm) for VIS (0.55–0.75 mm) channel of INSAT- 3D/-3DR imager and MODIS SWIR band (1.628–1.652 mm) for SWIR band (1.55–1.70 mm) of INSAT-3D/3DR imager. In order to estimate the uncertainty due to BRDF on TOA spectral radiance, 6SV RT model was run with and without BRDF. BRDF impact on TOA spectral radiances is discussed further in the section of error budget.

3.2 Statistical analyses

Statistical analyses are carried out for the additional information on how accurately the satellite measurement agrees with simulated values using in-situ measurements. Thus, the Root Mean Square Error (RMSE) to characterize the bias of algorithms in absolute terms is computed using Eq. (3):

$$RMSE = \frac{\sqrt{\frac{1}{n}\sum_1^n (estimated - measured)^2}}{\frac{1}{n}\sum_1^n (mesured)} \quad (3)$$

The percentage of relative error (RE) to describe the bias of algorithms (negative, if algorithm under estimates; positive, if it over estimates) is computed using the following equation:

$$RE = \frac{(estimated - measured)}{measured} \times 100 \quad (4)$$

Linear regression of the INSAT-3D/-3DR measured radiance and 6SV simulated radiance as well as 6SV simulated reflectance and ground measured reflectance are also generated, for which the coefficient of determination (R^2) were inspected.

4. Results and Discussion

4.1 TOA spectral radiance Comparison

Fig.-6 shows the results of linear regression of TOA spectral radiance for VIS and SWIR bands of INSAT-3DR (a-b) and INSAT-3D (c-d). In order to compare the radiance, we have averaged the *in-situ* points that covered within the single pass of satellite and similarly the nearest pixel from satellite are averaged and compared the single value per overpass. As per Table-1, we have total 28 overpass for INSAT-3D and 29 for INSAT-3DR. Therefore, the total number of points in the scatter plot (Fig.-6) are 29 for INSAT-3DR (a-b) and 28 for INSAT-3D (c-d). The results indicate good statistical agreement between INSAT-3DR derived TOA spectral radiance and 6SV simulated TOA spectral radiance, with R^2 values of 0.93 and 0.88 for VIS and SWIR respectively. The estimated RMSE values are found to be small 3 $Wm^{-2}sr^{-1}\mu m^{-1}$ and 1.09 $Wm^{-2}sr^{-1}\mu m^{-1}$ for VIS and SWIR respectively. The bias between satellite derived radiance and 6SV simulated radiance are very minimal, with the values of 2.50 $Wm^{-2}sr^{-1}\mu m^{-1}$ and 0.82 $Wm^{-2}sr^{-1}\mu m^{-1}$ for VIS and SWIR bands of INSAT-3DR respectively. The correlation is found better in VIS as compared to SWIR may be caused by variation in surface moisture, which vary with time. Contrary, the statistical agreement between INSAT-3D and 6SV simulated TOA spectral radiance is found to be moderate with R^2 value of 0.69 and 0.68 (VIS and SWIR) with a large bias value of 18.04 and 2.25 $Wm^{-2}sr^{-1}\mu m^{-1}$ (VIS and SWIR) as

compared to INSAT-3DR. The estimated RMSE is also found to be large 5.66 $Wm^{-2}sr^{-1}\mu m^{-1}$ and 1.67 $Wm^{-2}sr^{-1}\mu m^{-1}$ for VIS and SWIR respectively. On average, relative error (RE) between 6SV simulated and INSAT-3DR derived TOA spectral radiance are 0.93% and 0.85% for VIS and SWIR, respectively, while in the case of INSAT-3D, the RE is found to be much large with the values of 30% and -8.5% for VIS and SWIR, respectively.

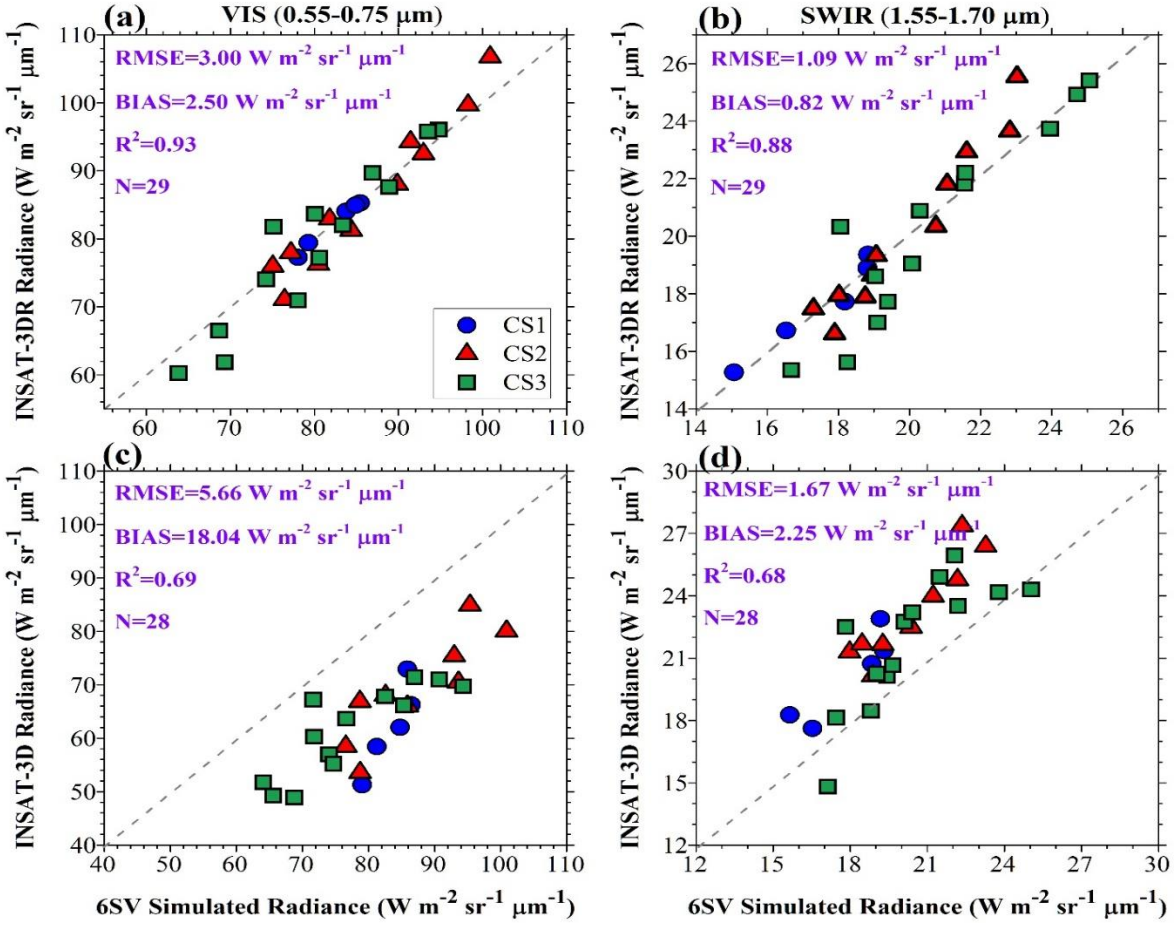

Figure 6: *Comparison between 6SV simulated TOA spectral radiance vs. measured TOA spectral radiance of INSAT-3DR (a-b) and INSAT-3D (c-d) for VIS and SWIR bands.*

Fig.-7 illustrates the temporal results of 6SV simulated and INSAT-3D/-3DR measured TOA spectral radiance for VIS and SWIR with time. It is found that the difference (6SV - INSAT) between INSAT-3DR and 6SV simulated TOA spectral radiance is very small for both the bands over all three calibration sites. The difference found to be 0.1, 0.8 and 0.2 $Wm^{-2}sr^{-1}\mu m^{-1}$ in VIS and -0.1, 0.39 and -0.26 $Wm^{-2}sr^{-1}\mu m^{-1}$ in SWIR for CS-1, CS-2 and CS-3, respectively. The difference in radiance is found to be large for CS-2 compared to other two sites because of relatively large spatial variation of CS-2. CS-3 shows the quite large radiance difference than the CS-1 due to different in time period consider for the in-situ data collection over CS-3. The mean difference is found to be 0.45 $Wm^{-2}sr^{-1}\mu m^{-1}$and 0.05 $Wm^{-2}sr^{-1}\mu m^{-1}$ for VIS and SWIR, which indicates the INSAT-3DR measured TOA spectral radiance is slightly underestimates the 6SV simulate radiance.

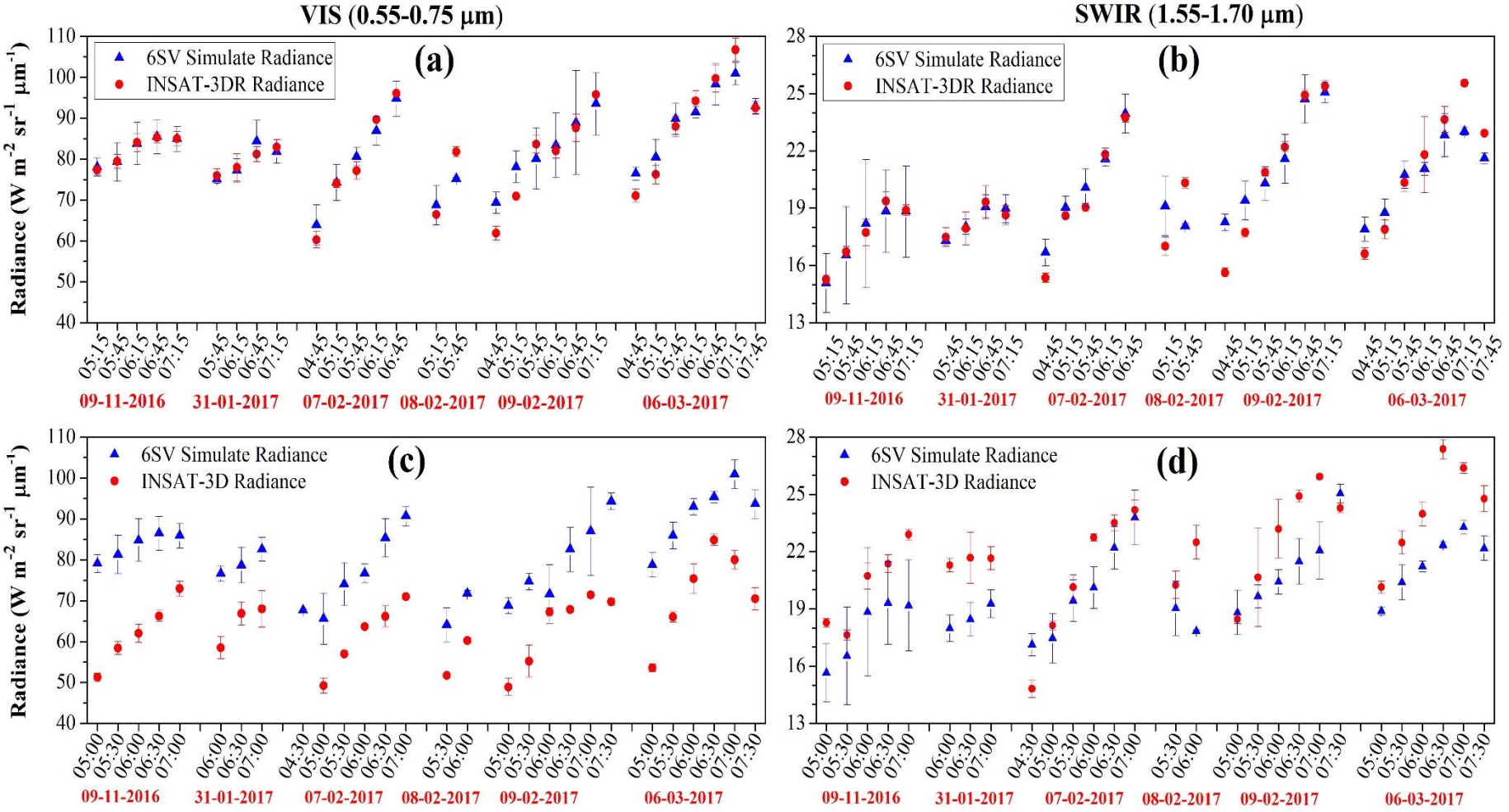

Figure 7: *Time series comparison of 6SV simulated TOA spectral radiance and INSAT-3DR (a-b) and INSAT-3D (c-d) measured TOA spectral radiance for VIS and SWIR channels over all calibration sites. The standard deviation bars are at 1σ level.*

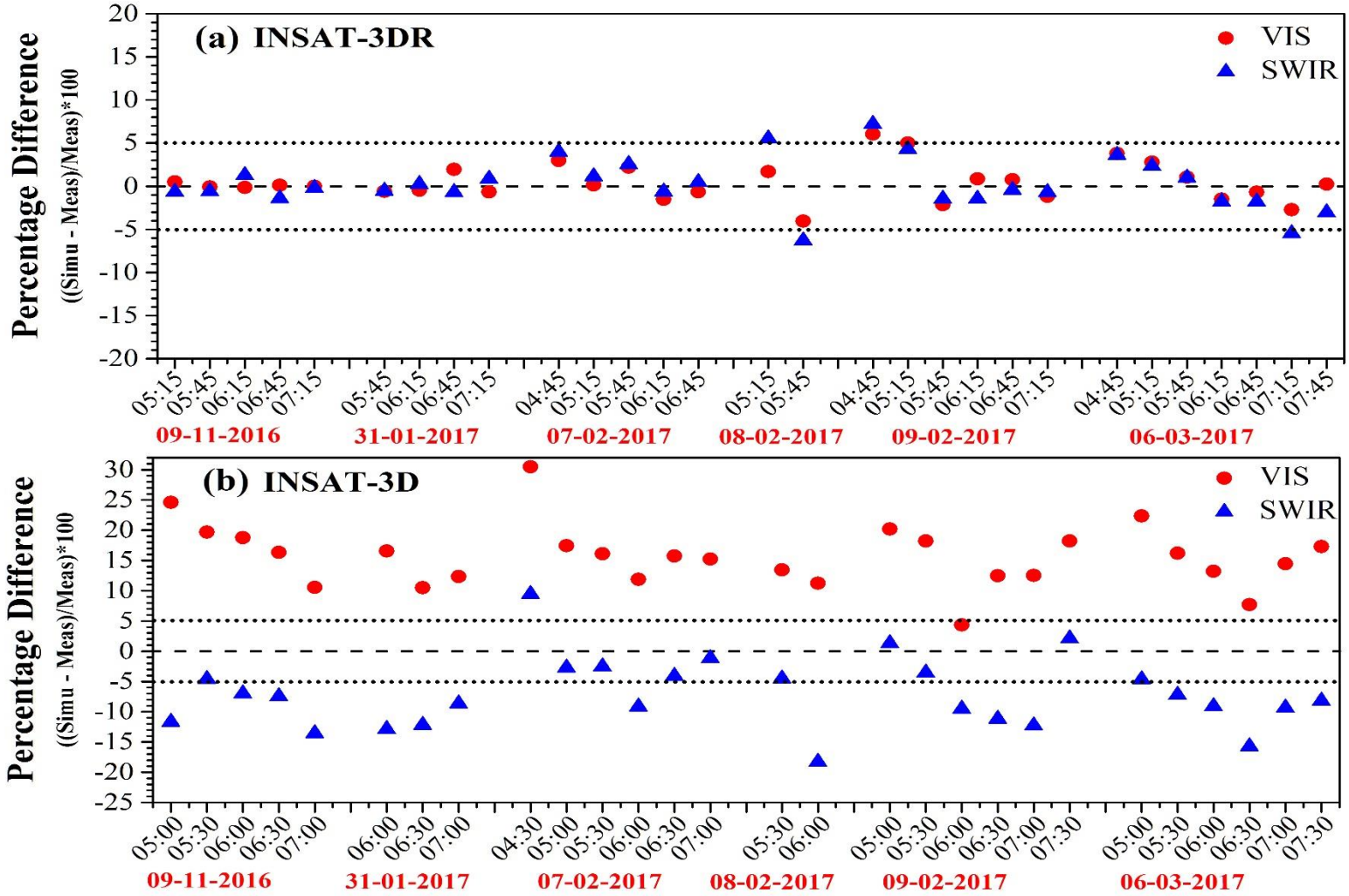

Figure 8: *Percentage difference in radiance between simulated and measured for VIS and SWIR of INSAT-3DR (a) and INSAT-3D (b).*

However, the difference between INSAT-3D and 6SV are found to be much larger for both the bands, as seen in fig.-7(c-d). The difference found to be 21.3, 16.9 and 17.9 $Wm^{-2}sr^{-1}\mu m^{-1}$ in VIS and -2.3, -1.4 and -2.86 $Wm^{-2}sr^{-1}\mu m^{-1}$ in SWIR for CS-1, CS-2 and CS-3, respectively. The mean difference is found to be 18.1 $Wm^{-2}sr^{-1}\mu m^{-1}$and -2.0 $Wm^{-2}sr^{-1}\mu m^{-1}$ for VIS and SWIR, which indicates the INSAT-3D measured TOA spectral radiance is underestimating the 6SV simulate radiance in VIS channel, while it is overestimating in SWIR bands.

Fig.-8 describes the results as the percentage difference in the TOA spectral radiance from simulation by 6SV as compared to satellite. In this case, 6SV simulation is considered as reference, so the percentage difference is given by

$$Percentage\ Difference = ((simulated - measured)/simulated) * 100 \qquad (5)$$

Where, measured are the satellite-based data. The results from all three desert sites agree with the INSAT-3DR (Fig,-8a) to within the uncertainties of the methods, which are on the order of 0.47% and 0.25% for VIS and SWR. There are points cross the values more than 5% especially over CS-2 during 9 February may be caused by the large solar zenith angle, while the contamination of very thin cirrus cloud at high altitude increase the percentage difference during 8 February over CS-2. Fig.-8(b) shows the percentage difference between 6SV simulated and INSAT-3D measured TOA spectral radiance. The results shows the large percentage difference for both VIS and SWIR bands, with the values of 15.6% and -7.1%, respectively. The overall results shows the INSAT-3D values are underestimate the 6SV simulated radiance in VIS band and overestimate in SWIR band.

4.2 Vicarious Calibration Coefficient

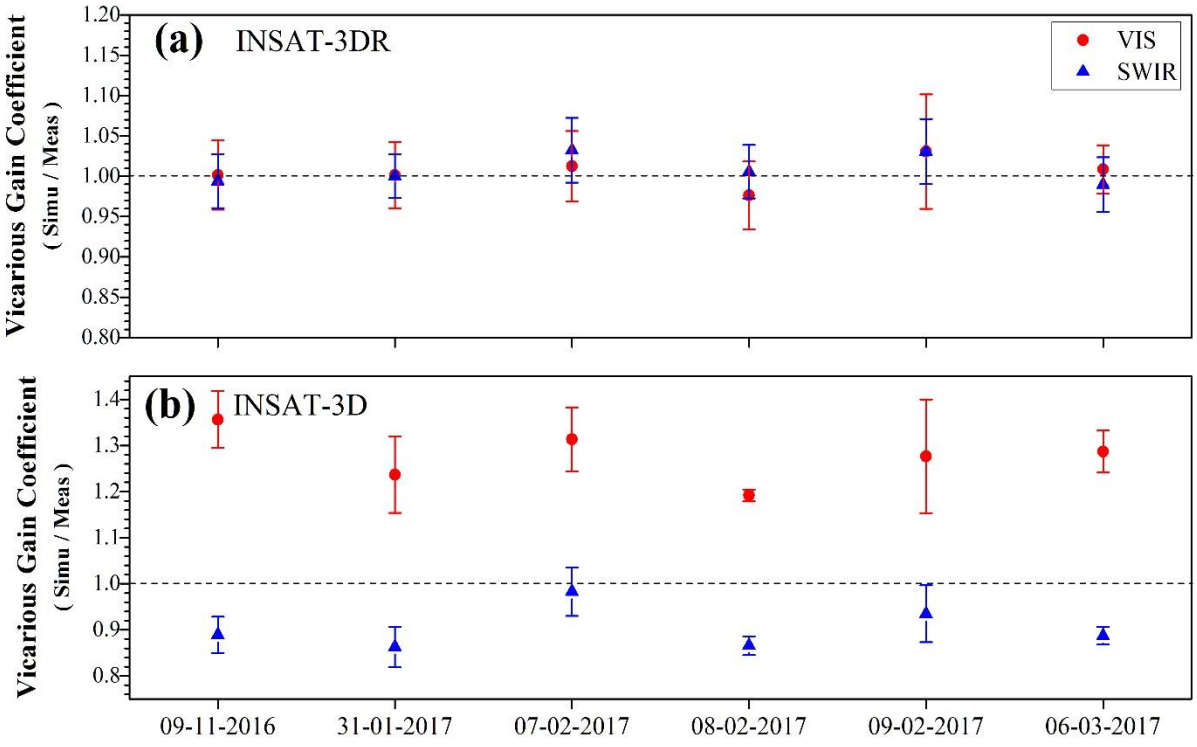

Figure 9: *Daily mean temporal variation of vicarious gain (calibration) coefficient for VIS nad SWIR of INSAT-3DR (a) and INSAT-3D (b).*

Table 4: *Vicarious calibration coefficients of VIS and SWIR channels of both INSA-3D/-3DR for all the period of time.*

Date	INSAT-3D			INSAT-3DR		
	Overpass Time	Calibration Coefficients		Overpass Time	Calibration Coefficients	
		VIS	SWIR		VIS	SWIR
09-11-2016	05:00/10:30	1.541425	0.8568	05:15/10:45	1.0099	0.9870
	05:30/11:00	1.391138	0.9382	05:45/11:15	0.9982	0.9884
	06:00/11:30	1.366783	0.9090	06:15/11:45	0.9970	1.0261
	06:30/12:00	1.304896	0.9037	06:45/12:15	1.0024	0.9725
	07:00/12:30	1.177531	0.8376	07:15/12:45	0.9994	0.9960
31-01-2017	06:00/11:30	1.3124	0.8446	05:45/11:15	0.9884	0.9898
	06:30/12:00	1.1776	0.8538	06:15/11:45	0.9913	1.0069
	07:00/12:30	1.2204	0.8910	06:45/12:15	1.0386	0.9871
	-	-	-	07:15/12:45	0.9870	1.0174
07-02-2017	04:30/10:00	1.4711	1.1562	04:45/10:15	1.0585	1.0871
	05:00/10:30	1.3349	0.9627	05:15/10:45	1.0034	1.0234
	05:30/11:00	1.3001	0.9664	05:45/11:15	1.0443	1.0537
	06:00/11:30	1.2046	0.8845	06:15/11:45	0.9693	0.9879
	06:30/12:00	1.2922	0.9443	06:45/12:15	0.9867	1.0094
	07:00/12:30	1.2778	0.9833	-	-	-
08-02-2017	05:30/11:00	1.1920	0.9388	05:15/10:45	1.0334	1.1231
	06:00/11:30	1.1912	0.7926	05:45/11:15	0.9192	0.8883
09-02-2017	05:00/10:30	1.4074	1.0198	04:45/10:15	1.1211	1.1686
	05:30/11:00	1.3981	0.9658	05:15/10:45	1.1005	1.0947
	06:00/11:30	1.0659	0.8803	05:45/11:15	0.9566	0.9716
	06:30/12:00	1.2168	0.8624	06:15/11:45	1.0174	0.9714
	07:00/12:30	1.2182	0.8506	06:45/12:15	1.0117	0.9915
	07:30/13:00	1.3525	1.0310	07:15/12:45	0.9762	0.9865
06-03-2017	05:00/10:30	1.4701	0.9378	04:45/10:15	1.0763	1.0783
	05:30/11:00	1.3010	0.9065	05:15/10:45	1.0552	1.0486
	06:00/11:30	1.2343	0.8853	05:45/11:15	1.0208	1.0199
	06:30/12:00	1.1242	0.8166	06:15/11:45	0.9706	0.9721
	07:00/12:30	1.2608	0.8824	06:45/12:15	0.9859	0.9649
	07:30/13:00	1.3299	0.8952	07:15/12:45	0.9456	0.9014
	-	-	-	07:45/13:15	1.0050	0.9427

The vicarious calibration coefficient is the ratio of 6SV simulated radiance and satellite observed radiance. For an ideal case, if there is no degradation in the sensor during launch and if the ground and atmosphere are properly characterized and the RT code is perfect then the simulated TOA spectral radiance and the satellite observed radiance should match precisely with each other. It means the ratio of simulated to observe radiance should be unity. In practice it is not possible, there are uncertainties in field reflectance and atmospheric measurements, modelling uncertainties in the RT code. To evaluate the coefficients and describe the characteristics of the INSAT-3D/-3DR observed radiances, we compared the vicarious calibration coefficients derived for VIS and SWIR in Fig.-9. Table-4 shows the vicarious calibration coefficients of VIS and SWIR channels of INSAT-3D/-3DR for a period of time.

The result reveals a very small deviation in vicarious calibration coefficients from unity for the VIS and SWIR bands of INSAT-3DR (fig.-9(a)) indicating its stability with very less degradation. The mean vicarious calibration coefficients are found to be 1.005 and 1.088 for VIS and SWIR bands of INSAT-3DR, respectively. The change in vicariously calibration coefficient are relatively high in the case of INSAT-3D. The mean vicarious calibration coefficient are found to be 1.277 and 0.903 for VIS and SWIR bands of INSAT-3D, respectively. This clearly indicates the large degradation in VIS and SWIR bands of INSAT-3D. In the conclusion, the noted values are found to be consistent for INSAT-3DR, which indicate good calibration stability of INSAT-3DR VIS and SWIR bands, while the values for INSAT-3D VIS and SWIR channels indicate the large degradation in the sensor.

4.3 Error Budget

The calibration uncertainty in the reflectance-based approach has been discussed in the earlier work [21], [35]. Recently, the uncertainty is reassessed and improved uncertainty in the reflectance based approach is estimated 73% in the middle of the visible portion of the spectrum [36]. The simulated TOA spectral radiance depends on many variables like atmospheric parameters, surface reflectance measurements, solar and viewing geometry, which directly affects the accuracy of calibration. The dependence of TOA spectral radiance on these variables is complex and it is difficult to quantify it in a closed, analytical form.

(1) The important source of uncertainty is dominated by the laboratory determination of the reference panel. We have maintained the Spectralon diffuse reflectance standard, which is calibrated and traceable to the NIST. It is used as a laboratory standard to which the field panels are compared prior to the campaign. The recently estimated uncertainty in the laboratory panel measurement is to be 1.5% to 1.7% in the VIS and SWIR region.
(2) The uncertainty in the surface reflectance spectra is due to variability in the surface characteristics. This uncertainty is estimated by calculating the CV at each band and for each site. The mean CV are found to be 7.1%, 9.1% and 3.9% for VIS and 10.2%, 6.9% and 3.0% for SWIR of CS-1, CS-2 and CS-3, respectively.
(3) In addition, the uncertainty that is caused by the 6SV model. The estimated accuracy for 6SV RT code is much improved compared to the earlier version and the relative error is estimated as 0.4–0.6% [29], [37] according to the error transfer theory.
(4) In practise, it is difficult to accurately determine aerosol properties in field experiments. In the present study, the aerosol type analysis confirms the selection of the optimum aerosol model. Then again two other aerosol types (i.e. urban aerosols and desert aerosol) are chosen to replace the continental aerosol model in order to approximate their

contributions to the systematic calibration uncertainty. We have re-calculated the calibration coefficients using 6SV RT code with different aerosol types. It is evident that the reflectance-based method is more sensitive to aerosol type than the other methods. The relative errors are 1.12% and 1.11% for VIS and SWIR respectively, using desert aerosol model and 2.15% and 2.14% for VIS and SWIR, respectively, using urban aerosol model.

(5) The Bi-directional Reflectance Distribution Function (BRDF) effect is adding an uncertainty into calibration coefficient, which is one of the important steps in calibration. The effect of surface reflectance anisotropy is assessed by estimating TOA spectral radiance with the BRDF coefficients (using MODIS BRDF product) for a site and comparing this with TOA spectral radiance computes using surface measurements. The estimated uncertainty due to BRDF effect is 0.52% for VIS and 0.88% for SWIR.

(6) The estimated uncertainty due to measurements of aerosol optical depth, total columnar ozone and columnar water vapour is 1.2%, 1.5% and 1.7%, respectively.

Table 5: *Estimated uncertainty in the reflectance-based approach for VIS and SWIR channels*

Source of Uncertainty	**VIS (%)**	**SWIR (%)**
Surface Reflectance Measurements		
Spectralon panel calibration	1.6	1.6
Ground measurements errors		
CS-1	7.1	10.2
CS-2	9.1	6.9
CS-3	3.9	3.0
Absorption computation		
Total Columnar Ozone	1.5	1.5
Columnar Water Vapour	1.7	1.7
Optical depth measurements	1.2	1.2
Selection of aerosol types[a]	1.12	1.11
Uncertainty due to BRDF effect	0.52	0.88
Inherent code accuracy	0.6	0.6
Total Uncertainty (root sum of squares)[b]	**4.99**	**4.33**

For the total uncertainty, **[a]**only the uncertainty due to desert model is considered and **[b]**only the CS-3 is considered.

Table-5 shows the estimated uncertainty in the reflectance-based approach for VIS and SWIR bands. From the error analysis, the total uncertainty is estimated 4.99% for VIS and 4.33% for SWIR.

5. Conclusion

In the present study, post-launch calibration is carried out to monitor the radiometric calibration stability of VIS and SWIR channels of INSAT-3D/-3DR over three different desert sites over a period of time. The TOA spectral radiance is simulated by 6SV RT model using ground measurements to compare with the measured TOA spectral radiance from INSAT-3D/-3DR. The conclusions based on this study are summarised below:

(1) The spatial variation of all three desert sites are quantified by coefficient of variation (CV) is found 7.1%, 9.1% and 3.9% for VIS and 10.2%, 6.9% and 3.0% for SWIR of CS-1, CS-2 and CS-3, respectively. This indicates the CS-3 is highly uniform site and more reliable for post-launch vicarious calibration.
(2) The 6SV simulated radiances are in good agreement with the INSAT-3DR measured radiance for all three calibration sites but shows the averaged agreement with INSAT-3D measured radiance.
(3) The percentage difference in radiance is found to be 0.47% and 0.25% for VIS and SWIR of INSAT-3DR respectively, whereas it was 15.6% and -7.1% for VIS and SWIR of INSAT-3D, respectively. This shows the underestimation of VIS and overestimation of SWIR bands of INSAT-3D.
(4) Vicarious calibration coefficients are computed to be 1.005 and 1.088 for VIS and SWIR of INSAT-3DR, respectively, while 1.277 and 0.903 for VIS and SWIR of INSAT-3D, respectively, indicates a significant change in VIS and SWIR bands of INSAT-3D which is suggested to be incorporated in generating next level of data products.
(5) The estimated total uncertainty in the computed calibration coefficients is found to be 4.99% in VIS and 4.33% in SWIR, respectively.

Acknowledgement

The authors gratefully acknowledge the encouragement received from Director, SAC for carrying out the present research work. Valuable suggestions received from Deputy Director, EPSA are also gratefully acknowledged. Authors are also thankful to the Cal-Val team member for their supports.

References

[1] S. Belward, "International co-operation in satellite sensor calibration; the role of the GEOS working group on calibration and validation," Adv. Space Res., vol. 23, no. 8, pp. 1443–1448, Jan. 1999.
[2] S. Liang, Quantitative Remote Sensing of Land Surface. New York, NY, USA: Wiley, 2004, pp. 178–194.
[3] J. J. Butler and R. A. Barnes, "Calibration strategy for the Earth Observing System (EOS)- AM1 platform," IEEE Trans. Geosci. Remote Sens., vol. 36, no. 4, pp. 1056–1061, Jul. 1998.
[4] H. S. Chen, Remote Sensing Calibration Systems: An Introduction. Hampton, VA, USA: Deepak, 1997.
[5] M. Dinguirard and P. N. Slater, "Calibration of space-multispectral imaging sensors: A review," Remote Sens. Environ., vol. 68, no. 3, pp. 194–205, Jun. 1999.
[6] O. Hagolle et al., "Results of POLDER in-flight calibration," IEEE Trans. Geosci. Remote Sens., vol. 37, no. 3, pp. 1550–1566, May 1999.

[7] W. A. Abdou et al., "Vicarious calibration experiment in support of the multi-angle imaging spectroradiometer," IEEE Trans. Geosci. Remote Sens., vol. 40, no. 7, pp. 1500–1511, Jul. 2002.
[8] D. X. Kerola, C. J. Bruegge, H. N. Gross, and M. C. Helmlinger, "Onorbit calibration of the EO-1 Hyperion and Advanced Land Imager (ALI) sensors using the LED Spectrometer (LSpec) automated facility," IEEE Trans. Geosci. Remote Sens., vol. 47, no. 4, pp. 1244–1255, Apr. 2009.
[9] A. Kamei et al., "Cross calibration of FORMOSAT-2 Remote Sensing Instrument (RSI) using Terra Advanced Spaceborne Thermal Emission and Reflectance Radiometer (ASTER)," IEEE Trans. Geosci. Remote Sens., vol. 50, no. 11, pp. 1–11, Nov. 2012.
[10] C.-C. Liu et al., "Vicarious calibration of the FORMOSAT-2 remote sensing instrument," IEEE Trans. Geosci. Remote Sens., vol. 48, no. 4, pp. 2162–2169, Apr. 2010.
[11] S. B. Seo, "Relative compensation method for degradation of visible detectors using improved direct histogram specification," Electron. Lett., vol. 50, no. 6, pp. 446–447, Mar. 2014.
[12] K. J. Thome, S. F. Bigger, and W. Wisniewski, "Cross comparison of EO-1 sensors and other Earth resources sensors to Landsat-7 ETM+ using Railroad Valley Playa," IEEE Trans. Geosci. Remote Sens., vol. 41, no. 6, pp. 1180–1188, Jun. 2003.
[13] M. Pagnutti et al., "Radiometric characterization of IKONOS multispectral imagery," Remote Sens. Environ., vol. 88, no. 1/2, pp. 53–68, Nov. 2003.
[14] P. Patel, H. Bhatt, A. K. Shukla, "Absolute vicarious calibration of recently launched Indian meteorological satellite: INSAT-3D imager." ISPRS technical Commission VIII symposium, Hyderabad, India, 09– 12 December 2014. http://dx.doi.org/10.5194/isprsarchives-XL-8-291-2014.
[15] P.N. Patel, H. Bhatt, A. K. Mathur, R. P. Prajapati, G. Tyagi, "Reflectance-based vicarious calibration of INSAT-3D using high-reflectance ground target." Vol. 3, pp. 20-35. Dec. 2015.
[16] INSAT-3D Data Products Format Document, 2014. Version 1.1. SAC/IMDPS/ SIPA/DPSG/MSDPD/TN-01/FEB 2014. ⟨www.mosdac.gov.in/Missions/ docs/INSAT3D_Products.pdf⟩.
[17] Chander, G., Xiong, X., Choi, T., Angal, A., 2010. Monitoring on-orbit calibration stability of the Terra MODIS and Landsat 7 ETMþ sensors using pseudo-invariant test sites. Remote Sens. Environ. 114, 925–939.
[18] Bouvet, M., 2014. Radiometric comparison of multispectral imagers over a pseudo-invariant calibration site using a reference radiometric model. Remote Sens. Environ. 140, 141–154.
[19] Teillet, P., Chander, G., 2010. Terrestrial reference standard sites for post-launch sensor calibration. Can. J. Remote Sens. 36, 437–450.
[20] Scott, K.P., Thome, K.J., Brownlee, M., 1996. Evaluation of the railroad valley playa for use in vicarious calibration. Proc. SPIE 2818, 158–166.
[21] Slater, P.N., Biggar, S.F., Thome, K.J., Gellman, D.I., Spyak, P.R., 1996. Vicarious radiometric calibrations of EOS sensors. J. Atmos. Ocean. Technol. 13, 349–359.
[22] Slater, P.N., Biggar, S.F., Holm, R.A., Jackson, R.D., Mao, Y., Moran, M.S., Palmer, J.M., Yuan, B., 1987. Reflectance- and radiance-based methods for in-flight absolute calibration of multispectral sensors. Remote Sens. Environ. 22, 11–37.
[23] Teillet, P.M., Horler, D., O'Neill, N.T., 1997. Calibration, validation, and quality assurance in remote sensing: a new paradigm. Can. J. Remote Sens. 23 (4), 401–414.
[24] Reagan, J.A., Thomason, L.W., Herman, B.M., Palmer, J.M., 1986. Assessment of atmospheric limitations on the determination of the solar spectral constant from ground-based spectroradiometer measurements. IEEE Trans. Geosci. Remote Sens. GE-24, 258– 266.
[25] Schmid, B., Wehrli, C., 1995. Comparison of sun photometer calibration by use of the Langley technique and standard lamp. Appl. Opt. 34, 4500–4512.
[26] Morys, M., Mims III, F.M., Hagerup, S., Anderson, S.E., Baker, A., Kia, J., Walkup, T., 2001. Design, calibration, and performance of MICROTOPS II handheld ozone monitor and Sun photometer. J. Geophys. Res. 106 (D13), 14573–14582.

[27] Porter, J.N., Miller, M., Pietras, C., Motell, C., 2001. Ship-based Sun photometer measurements using microtops Sun photo-meters. J. Atmos. Ocean. Technol. 18, 765–774.
[28] Gellman, D.I., Biggar, S.F., Slater, P.N., Bruegge, C.J., 1991. Calibrated intercepts for solar radiometers used in remote sensor calibration. Proc. SPIE 1493, 19–24.
[29] Kotchenova, S.Y., Vermote, E.F., Levy, R., Lyapustin, A., 2008. Radiative transfer codes for atmospheric correction and aerosol retrieval: intercomparison study. Appl. Opt. 47 (13), 2215–2226.
[30] Vermote, E.D., Tanre, J.L., Deuze, M., Herman, J.J., Morcrette, Kotchenova, S.Y., 2006. Second Simulation of Satellite Signal in the Satellite Spectrum (6S). 6S User Guide Version 3. University of Maryland.
[31] Markham, B.L., Halthore, R.N., Goetz, S.J., 1992. Surface reflectance retrieval from satellite and aircraft sensors: results of sensor and algorithm comparison during FIFE. J. Geophys. Res. 97. (D17718), 7857795.
[32] Nicodemus, F.E., Richmond, J.C., Hsia, J.J., Ginsberg, I.W., Limperis, T., 1977. Geometrical considerations and nomenclature for reflectance. Natl. Bur. Stand. Rep. NBS MN-160, 52.
[33] P. Nandy, K. Thome, and S. Biggar, "Characterization and field use of a CCD camera system for retrieval of bidirectional reflectance distribution function," J. Geophys. Res., vol. 106, no. D11, pp. 11 957–11 966, 2001.
[34] MODIS ATBD. 1999. Strahler, A.H., Muller, J.P., MODIS BRDF/Albedo Product, Algorithm Theoretical Basis Document, Version 5, April 1999.
[35] Thome, K.J., 2001. Absolute radiometric calibration of Landsat 7 ETM+ using the reflectance-based method. Remote Sens. Environ. 78, 27–38.
[36] Czapla-Myres, J., McCorkel, J., Anderson, N., Thome, K., Biggar, S., Helder, D., Aaron, D., Liegh, L., Mishra, N., 2015. The ground-based absolute radiometric calibration of Landsat 8 OLI. Remote Sens. 7, 600–626, http://dx.doi.org/10.3390/rs/0100600.
[37] Chen, Z., Zhang, B., Zhang, H., Zhang, W., 2014. Vicarious calibration of Beijing-1 multispectral imagers. Remote Sens. 6, 1432–1450, http: //dx.doi.org/10.3390/rs6021432.